

Probing liquid surface waves, liquid properties and liquid films with light diffraction

Tarun Kr. Barik, Partha Roy Chaudhuri, Anushree Roy and Sayan Kar*

Department of Physics, Indian Institute of Technology, Kharagpur 721 302, India

Abstract

Surface waves on liquids act as a dynamical phase grating for incident light. In this article, we revisit the classical method of probing such waves (wavelengths of the order of mm) as well as inherent properties of liquids and liquid films on liquids, using optical diffraction. A combination of simulation and experiment is proposed to trace out the surface wave profiles in various situations (*eg.* for one or more vertical, slightly immersed, electrically driven exciters). Subsequently, the surface tension and the spatial damping coefficient (related to viscosity) of a variety of liquids are measured carefully in order to gauge the efficiency of measuring liquid properties using this optical probe. The final set of results deal with liquid films where dispersion relations, surface and interface modes, interfacial tension and related issues are investigated in some detail, both theoretically and experimentally. On the whole, our observations and analysis seem to support the claim that this simple, low-cost apparatus is capable of providing a wealth of information on liquids and liquid surface waves in a non-destructive way.

PACS numbers: 42.25.Fx, 42.25.Hz, 42.30.Kq, 42.30.Lr, 05.70.Np, 68.05.-n

*Electronic address: sayan@phy.iitkgp.ernet.in

I. INTRODUCTION

Optical probes are usually non-destructive – they do not change the properties of the medium being probed in any significant way (unless the probe power is large). Diffraction and scattering of light, as is known over centuries, are therefore capable of providing a variety of information. In this article, we revisit a well-known classical method of investigating liquid surface waves using light diffraction. Although this method is well-studied in the context of measurements of surface tension of liquids [1], our motivation for revisiting it is primarily aimed at demonstrating its utility and capability in understanding a wider class of situations/phenomena. In particular, we investigate two aspects – surface wave profiles and liquid properties for waves on a single liquid and also for waves on liquid films.

Before we begin with details, it is worth summarizing some of the earlier work on liquid as well as solid surface waves. Use of laser light scattering is a unique technique for non-contact, noninvasive study of surface acoustic waves and capillary waves [2]. Technological advances directed toward diverse applications of surface acoustic waves on solid surfaces are now well established, and has resulted in important developments in the fabrication of practical devices [3, 4, 5, 6, 7, 8, 9, 10, 11].

However, relatively few articles deal with surface waves on liquid surfaces [12, 13, 14, 15, 16, 17, 18, 19, 20]. To mention a few, high frequency capillary waves at the surface of liquid gallium and the mercury liquid-vapor interface have been studied by means of quasi-elastic light-scattering spectroscopy [21]. The spatial damping coefficient of low-frequency surface waves at air-water interfaces, using a novel heterodyne light-scattering technique, has been measured and reported in [22]. Quasi-elastic light scattering has been used to study thermally excited capillary waves on free liquid surfaces over a considerably wider range of surface wavenumbers [13, 16]. Measurements of the decay coefficient of capillary waves in liquids covered with monolayers of stearic acid, oleyl alcohol, and hemicyanine are reported in [23]. Also, the measurement of the pressure-area compression isotherm in Langmuir monolayer films using the laser light diffraction from surface capillary waves is reported in [24].

In a recent article, we have shown how the effect of interfering waves on a liquid surface could be inferred from the nature of the diffraction pattern [15]. Here we begin by proposing a combined method of simulation and experiment, sufficiently general in nature and capable

of verifying the nature of the actual liquid surface wave profile. Having known the profile, we then focus on the dispersion relation and discuss experiments to determine the surface tension and viscosity of liquids. Finally, we turn to liquid films where we try to understand the profile through the various modes (surface and interface) and then go on to check the values of interfacial tension.

Section II describes the basic scheme of our experimental arrangement. The methodology of our experiment and typical results pertaining to the surface wave profile are discussed in section III. In section IV, we discuss theory, observations and measurements of surface tension and viscosity for different liquids. Section V first discusses the theoretical platform for surface capillary wave on liquid films. We then verify our theory with experiments. Finally, in section VI, we summarize our results with some concluding remarks.

II. EXPERIMENTAL DETAILS AND THE THEORETICAL BACKGROUND

A. Experimental setup

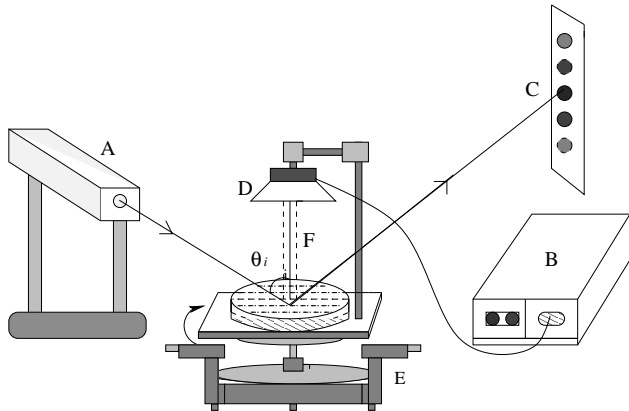


FIG. 1: Schematic diagram of the experimental setup to study capillary wave on liquid; A: Laser, B: Frequency generator, C: Screen, D: Loudspeaker, E: Spectrometer and prism table assembly and F: Exciter.

As shown in Fig. 1, a petridish of diameter about 18.5 cm is filled with the experimental liquid to a depth of ~ 1 cm. A metal pin with its blunt end glued vertically upright to the diaphragm of a loud speaker (held above the petridish) acts as an exciter. When slightly immersed in the liquid and driven by a low frequency sinusoidal signal generator, this exciter

vibrates vertically up and down and generates the desired liquid surface waves. To study the profile of surface waves we place the petridish-loud-speaker assembly on the prism-table of a spectrometer in order to choose the diffracting element at any position on the liquid surface and to record the corresponding position from the prism-table scale (with a least count of 0.1 degree). Light from a 5 mW He-Ne laser ($\lambda = 632.8$ nm) having a beam diameter of ~ 1.8 mm is directed to fall on the liquid surface at an angle of incidence of 77° (θ_i), as noted in our experiment. The laser beam incident on the dynamical phase grating formed on the liquid surface, produces Fraunhofer diffraction pattern which is observed on a screen placed at a fairly large distance (3.42 meters in our case) from the diffraction center. The images of the diffraction pattern are recorded using a digital camera (make Sony, DSC - P93, 5.1 mega pixels). Spurious noise in the image is removed using Photoshop software. The intensity across the diffraction spots are measured using a photo-detector operating in the linear dynamic range of the photo-currents' response to optical power. During our experiment, the room temperature recorded is 25°C .

B. Theoretical background

We discuss here, briefly, the diffraction mechanism which lies at the heart of all our experiments. When monochromatic light of wavelength λ is incident on a circular surface wave of frequency ω and wavevector K , the phase modulation produced by the surface wave is given as

$$\phi(x') = \frac{2\pi}{\lambda} \left[(2h \cos \theta_i) \sin \left(\omega t - \frac{Kx'}{\cos \theta_i} \right) \right] \quad (1)$$

where, the factor of $\cos \theta_i$ appears due to oblique incidence of the incident monochromatic light [11, 14, 15, 25]. The field strength E of the diffraction pattern can be estimated from the Fourier transform of the aperture function (in this case the surface wave produced by single exciter). The intensity of the diffraction patterns, obtained from EE^* , is given by [25, 26]

$$I(x') = \sum_n J_n^2(4\pi h \cos \theta_i / \lambda) \delta \left(\frac{x'}{\lambda z} - \frac{n}{\Lambda \cos \theta_i} \right) \quad (2)$$

where z is the horizontal distance between the location of the laser spot on the liquid surface and the screen and $\Lambda = \frac{2\pi}{K}$, is the wavelength of the surface wave. h is the amplitude of the surface wave. x' is the coordinate which measures the distance of the diffraction spots from a reference point (central spot) on the observation plane. J_n is the Bessel function of order

n and $\delta()$ denotes the Dirac delta function. The intensity distribution on the diffraction pattern vanishes at points where J_n is zero satisfying Eqn. 2. The quantity involving the Bessel function in this equation gives the magnitude of the intensity of diffraction spots for different orders n , while the positions of the spots are given by the delta function.

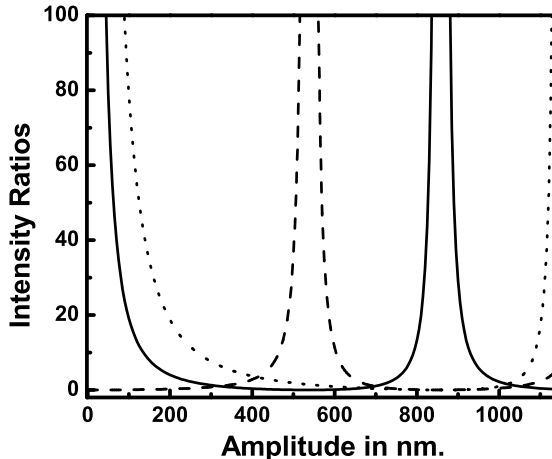


FIG. 2: Theoretical plot of wave amplitude versus intensity ratio for $\theta_i = 77^\circ$, $\lambda = 632.8$ nm. Solid line, dashed line and dotted line stand for the ratios I_0/I_1 , I_1/I_0 and I_0/I_2 respectively.

When we generate capillary waves by means of a single pin exciter, the amplitude of the wave at the point of oscillation is almost the same as the amplitude of the oscillating pin in a low viscous liquid [15]. The intensities of different orders depend only on the amplitude of the capillary wave (h), if other parameters like θ_i and λ are kept constant (Eqn. 2). Theoretical plots of wave amplitude versus the intensity ratios, I_0/I_1 , I_1/I_0 and I_0/I_2 , using Eqn. 2 (keeping θ_i and λ fixed) are shown in Fig. 2. In our experiment, for a particular ω , the intensity of different order spots in the diffraction pattern are measured by a photodiode detector when the laser beam is focused along a radial line on the liquid surface. The intensity ratios like I_0/I_1 and I_0/I_2 are then evaluated. By comparing our experimentally measured ratios with those obtained from the theoretical plot (Fig. 2), we estimate the average value of h . It is to be noted that, for $I_0 \ll I_1$, the value of this ratio I_0/I_1 becomes very small and could yield erroneous results. In such cases, we used the ratio I_1/I_0 for estimation of h (however, we were always below the limit for which this ratio becomes very large). Again, by measuring x' , we determined the wavelength (Λ) of the surface capillary

waves to be 2.1 mm [for more details see [15]]. For several exciters placed at different types of geometric configurations (eg, along a line, or a polygon etc.), the surface wave patterns change, and hence Eqn. 2 must also change.

III. THE SURFACE WAVE PROFILE

A. Simulation of the profile

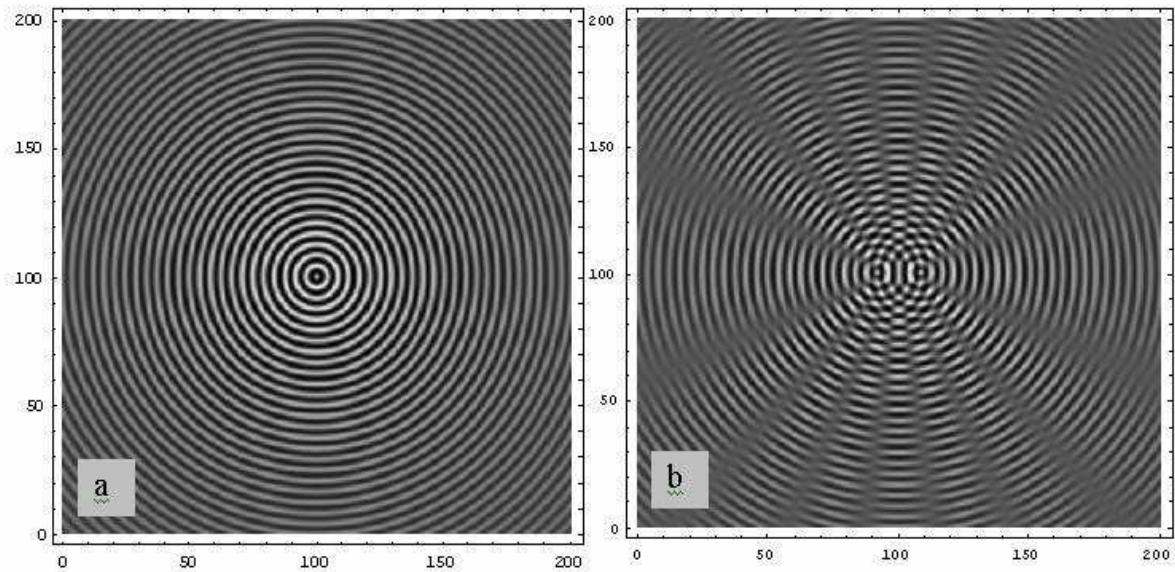


FIG. 3: The simulated surface capillary wave profiles for (a) single exciter and (b) two exciters.

Low frequency surface waves are not visible to the naked eye. One may appreciate this when we simulate the surface wave profile using realistic dimensions and parameters. In a previous study [15], we measured the surface-wave parameters (wavelength, amplitude at the point of excitation) at a given oscillation frequency (220 Hz). Here, we use similar typical values to generate theoretically the distribution of waves on the liquid surface. The equations, which we use to simulate the wave profile for the cases of single and double-pin exciters are (at a fixed time ‘ t ’, say $t=0$)

$$\psi_1(X, Y) = h \exp\left(-\delta\sqrt{(X - x_1)^2 + (Y - y_1)^2}\right) \cos\left(\frac{2\pi}{\Lambda}\sqrt{(X - x_1)^2 + (Y - y_1)^2}\right) \quad (3)$$

and

$$\psi_2(X, Y) = h \exp\left(-\delta\sqrt{(X - x_1)^2 + (Y - y_1)^2}\right) \cos\left(\frac{2\pi}{\Lambda}\sqrt{(X - x_1)^2 + (Y - y_1)^2}\right) + h \exp\left(-\delta\sqrt{(X - x_2)^2 + (Y - y_2)^2}\right) \cos\left(\frac{2\pi}{\Lambda}\sqrt{(X - x_2)^2 + (Y - y_2)^2}\right), \quad (4)$$

respectively. Here (x_1, y_1) and (x_2, y_2) are the centers of oscillations and δ is the spatial damping coefficient of the liquid. To mimic the intended experiments, we assume that each wave has the same frequency ω , wavelength Λ , and amplitude h (at the center of oscillation). In our simulations, we use the typical values of $\Lambda = 2.1$ mm, $h = 1.0$ mm and $D = 8.4$ mm (separation between pin-excitters) [15]. δ is chosen to be 0.235 cm^{-1} (for water at 220 Hz, we obtain this value from experiments discussed later in section IV). The corresponding surface-wave profiles estimated for the two cases of interest are shown in Fig. 3(a) and Fig. 3(b), respectively. Following this recipe one can obtain the surface-wave profile for any number of oscillation sources. The simulated profiles enable a better visualization, which, in turn, can act as a guideline for their actual experimental verification.

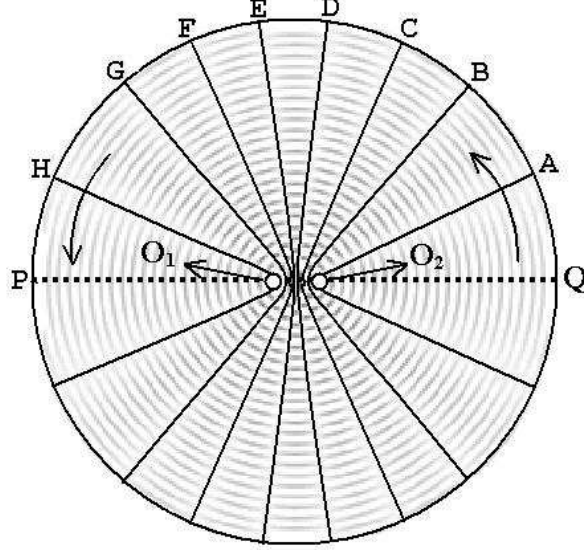


FIG. 4: The schematic of our experiment, which we have followed to verify the simulated two source pattern. O_1 and O_2 are the two excitters. Solid lines are the hyperbolic loci along the direction of destructive interference.

B. Experimental results for two source pattern

The simulated profiles are built on the assumptions made in Eqn. 3 and Eqn. 4. It is necessary to verify experimentally whether the assumptions are good enough to represent the characteristics of the surface waves. We note that the simulated two source interference pattern [shown in Fig. 3(b)] exhibits hyperbolic loci for the constructive and destructive interference nodes. Using this fact as a guideline, we trace the hyperbolic loci (maxima and minima of the interfering waves) on the liquid surface by observing the changes in the corresponding diffraction patterns. Initially, when the laser beam is incident along the central line PQ (see Fig. 4) where constructive interference of waves occur, the diffracted light shows, as expected [15], a central spot along with higher order ones symmetrically located on either side of the central spot [see Fig. 5(a)]. As we shift the probe beam gradually away from the central line along a circle (note the arrow in Fig. 4), the number of higher order spots progressively decreases till we reach the position of the adjacent hyperbola (O_2A), where the diffraction should ideally contain only the central order. In experiment, however, at this position, we find the first order spots too, though with very low intensity [see Fig. 5(b)]. This happens due to the finite spot size of the laser beam. Nevertheless, beginning with the central line at one side and gradually rotating the prism-table till we reach 180° , we observe a repetition of the patterns [shown in Fig. 5(a) and 5(b)] symmetrically at all complementary angles. We note the angular positions of all consecutive minima. These results are shown in Table-I. Thus, a comparison of our experiment (Fig. 4) with the simulation [upper half of Fig. 3(b)] for identical values of parameters shows the same number (eight) of destructive interference lines at almost the same angular separation. Beyond 180° and upto 360° , (*i.e.*, while scanning the lower semicircular region in Fig. 4) identical patterns are observed. This confirms that the Eqn. 4 used to describe and simulate the two source surface wave profile is, indeed, a correct representation of the observed profile. We note that our method of investigation is sufficiently general (we have indeed checked upto six exciters) and can be used for several exciters located along a line or in other geometric configurations (eg. exciters on a triangle, quadrilateral, pentagon, hexagon etc.).

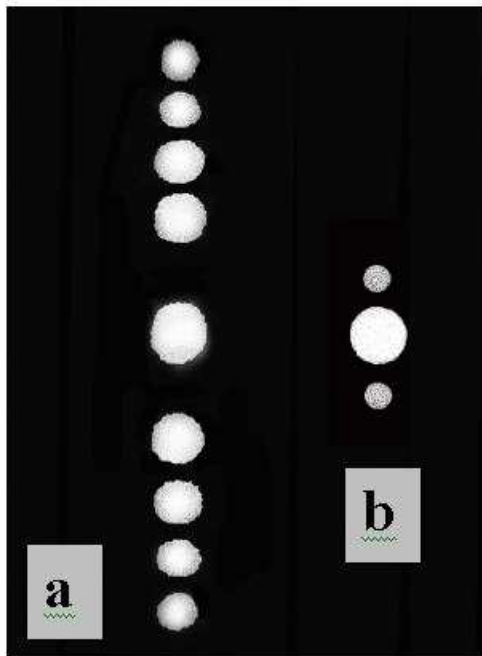


FIG. 5: Diffraction patterns when light is incident along the direction of (a) constructive interference and (b) destructive interference for the two source (exciter) case.

C. Minima distribution for oscillation sources in regular array

When multiple oscillating sources are used, different surface wave profiles can be generated by appropriately configuring their positions. It is interesting to study these interference patterns of the surface waves for multiple sources (e.g., a linear chain of oscillation sources or those placed in a closed regular geometric figure). A typical example of a simulated interference pattern for three oscillation sources is shown in Fig. 6. For this purpose, we choose to trace the distribution of minima lines in the simulated interference pattern in terms of the number of lines and their angular position. It is obvious that the number of minima lines increases with the increase in the number of oscillation sources. For example, our simulation of the pattern for 2, 3, 4, 5 and 6 oscillation sources placed in a straight line with a spacing of $D = 8.4$ mm between the adjacent two oscillators, and $\Lambda = 2.1$ mm, exhibits the number of hyperbolic lines respectively as 8, 16, 24, 32, and 40. To derive this behavior theoretically, we use the interference treatment for n -oscillating sources. We consider n (≥ 2) sources lying in a straight line. Representing the wave generated by each

oscillating source as $h \exp(i(\mathbf{K} \cdot \mathbf{r}_n - \omega t))$, where h is the amplitude and \mathbf{r}_n is the position vector from the n -th source to the point of observation, we find the resultant field ψ_P at a certain point P as [26],

$$\psi_p = h \frac{\text{Sin}(\frac{n\beta}{2})}{\text{Sin}(\frac{\beta}{2})} \exp(i(KR - \omega t)), \quad (5)$$

where $R = \frac{1}{2}D(n-1)\text{Cos}(\phi) + \mathbf{r}_1$, is the distance from the centre of the line of oscillators to the point P and $\beta = KDCos(\phi)$, is the phase difference between adjacent sources. Again ϕ is the angle between R and the line joining the sources of oscillation. For minima at P, the condition is $h \frac{\text{Sin}(\frac{n\beta}{2})}{\text{Sin}(\frac{\beta}{2})} = 0$. Using the boundary condition mentioned in [15], we calculate the allowed number of minima lines and their corresponding angular positions. For $n = 3$, for example, the above minima condition becomes $\frac{D}{\Lambda}\text{Cos}(\phi) = \pm(\frac{m}{2})$, where m is an integer but not equal to or multiple of n . If we choose $\frac{D}{\Lambda} = 4$, then $\text{Cos}(\phi)$ has only 16 allowed values, i.e. 16 hyperbolic minima lines are possible. The angular distribution of these asymptotic lines perfectly match with the observed pattern. We have carried out this comparison successfully for higher order n -values upto 5. From the above calculations we have seen that the number (N_o) of asymptotic minima lines in the region above (or below) the line joining the oscillation sources is directly proportional to the ratio $\frac{D}{\Lambda}$ and also the number of the interval $(n-1)$ between the exciters. Taking care of the \pm sign of $\text{Cos}(\phi)$, we can express N_o as

$$N_o = \frac{2D}{\Lambda} (n-1), \quad (6)$$

which gives the same result (for different n values) as obtained before. This relationship can, just by measuring the number of minima lines for given D and n , estimate Λ of the capillary waves.

Next we study n (≥ 3) oscillation sources forming a closed loop shape of an equilateral triangle, square, pentagon, and a hexagon. The number (N_c) of minima lines (which are lying on either side of a symmetric axis) in this case can be similarly expressed as,

$$N_c = \frac{2D}{\Lambda} \left(\frac{n}{2}\right), \quad (7)$$

The number of lines for the above stated closed geometrical figures at the same values of D and Λ are 12, 16, 20 and 24 respectively. We have not been able to calculate exactly the angular distribution of the minima lines. However, using the simulation mentioned above,

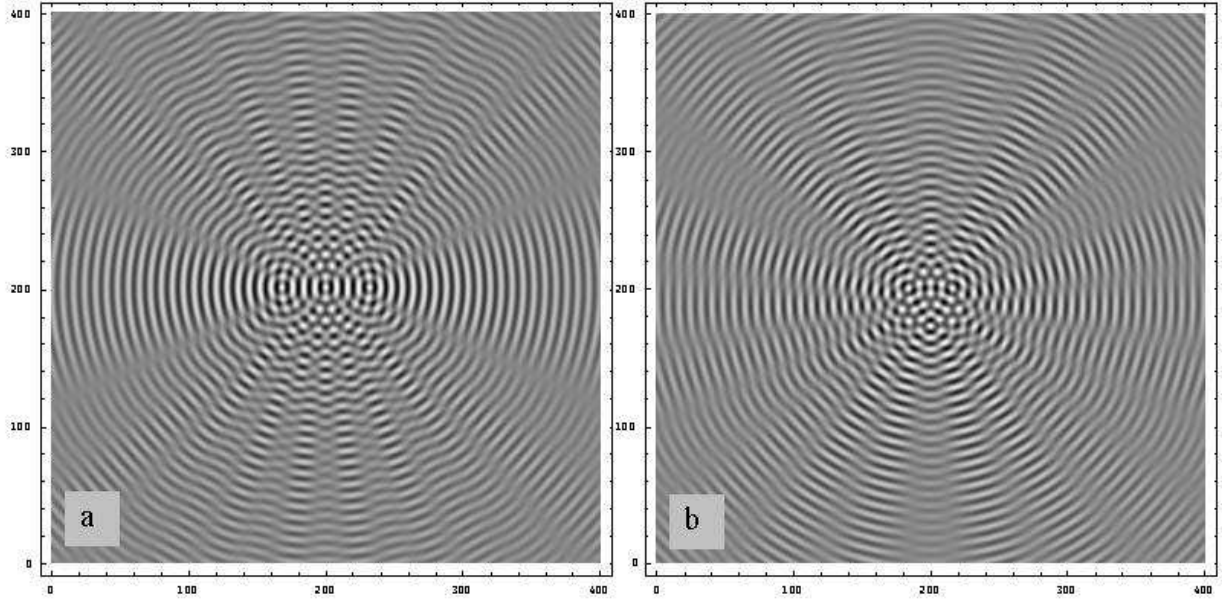


FIG. 6: Simulated interference profile of surface capillary wave for (a) three exciters in a straight line and (b) three exciters at the vertices of an equilateral triangle.

one can determine the interference pattern due to any number of oscillation sources placed along a line or at the vertices of polygons (regular or irregular). Such a study might be useful for generating a desired dynamic phase grating aperture for diffraction based micro-photonic systems.

IV. THE DISPERSION RELATION AND LIQUID PROPERTIES USING LIGHT DIFFRACTION

Knowing the surface wave profile is, of course, not enough. A crucial element of any wave phenomenon is the dispersion relation, which, obviously, contains within it, quantifiers of material properties (here, liquid properties, such as surface tension and viscosity). In this section we describe how we use Fraunhofer diffraction of laser light by the surface profile of ripples on liquids, described in Section III, to study such liquid properties. Several methods to accurately determine these two properties are now well-established and available in the literature. For measurement of surface tension, techniques widely used are the Capillary Rise method, Drop-weight method, Jaeger's method, Rayleigh's method etc. [27, 28]. Likewise, for the measurement of viscosity, popular methods like Poiseuille's method, Stokes' method

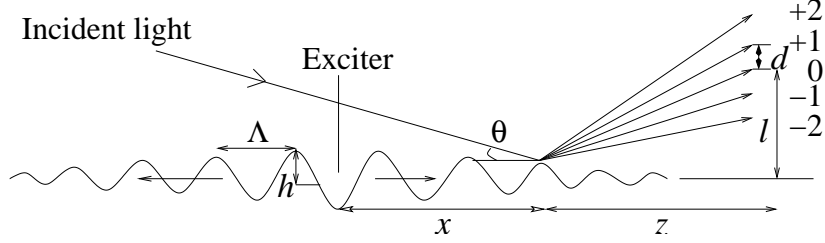


FIG. 7: Geometrical representation of the basic measurement on surface tension and viscosity.

etc., are well-known and gives accurate results [27, 28]. Here, we focus on a single optical set up which can measure both surface tension and viscosity of low-viscous liquids with reasonable accuracy. Though the measurement of surface tension of liquids using Fraunhofer diffraction of laser light by surface waves is well known in the literature [1], to the best of our knowledge the estimation of the viscosity of a liquid using this probe and, in particular, the simple method which we have followed, is certainly new. In the following we elaborate on the above mentioned measurements in some detail.

A. Surface tension

Consider the well-known dispersion relation for surface capillary wave on liquids [29, 30, 31]

$$\omega^2 = (gK + \alpha K^3/\rho). \quad (8)$$

Here ω and K are the angular frequency and wavevector of the surface capillary wave, respectively. α and ρ are the surface tension and density of the liquid and g is the acceleration due to gravity. The above relation shows that waves at the surface of the liquid are dominated by gravity as well as surface tension. Neglecting the gravitational effect and taking the logarithm on both sides of the Eqn. 8 we get

$$\ln \omega = \frac{3}{2} \ln K + \frac{1}{2} \ln \left(\frac{\alpha}{\rho} \right), \quad (9)$$

which is an equation of a straight line for $\ln \omega$ vs. $\ln K$ with a slope of $\frac{3}{2}$ and y-intercept $\frac{1}{2} \ln \left(\frac{\alpha}{\rho} \right)$, which contains the surface tension α .

In our experiments, we have generated the surface capillary wave on the liquid surface with a single exciter. As we discussed before, the expected surface wave profile [shown in Fig. 3(a)] acts as a reflection phase grating for the incident laser light and the intensity

distribution satisfies Eqn. 2. If we take the separation between the central order and the first order ($n=1$) diffraction spots to be d (see Fig. 7), then from the delta function in Eqn. 2 we get the expression for the wavenumber K as

$$K = \frac{2\pi d}{\lambda z} \sin\theta, \quad (10)$$

where $\theta = \frac{\pi}{2} - \theta_i$ is the grazing angle of incidence of the laser beam. For small grazing angle, we can approximate K as

$$K = \frac{2\pi l d}{\lambda z^2}, \quad (11)$$

where l is the perpendicular height of the central order spot from the liquid surface level (see Fig. 7). As ω changes, the distance between bright spots of the diffraction pattern also changes. Sets of diffraction patterns are obtained on the screen for different values of ω . For each set, we have traced the positions of spots of different order on the screen.

For Fraunhofer diffraction, values of z and l in Eqn. 11 are quite large (342 cm and 87 cm, respectively, in our experiment). Thus, the systematic error introduced in measuring these lengths with a metre scale (with a least count of 1.0 mm) is quite less. On the other hand, a careful and accurate measurement of d (of the order of few mm) is crucial for evaluating K . From the characteristic feature of the delta function in Eqn. 2, we find that the diffraction spots due to different orders are equidistant for a particular frequency of capillary wave. Thus, to reduce the systematic error in measuring d , we have measured the separation between the positive and the negative fourth-order (fifth-order) spots. The values of d are obtained through averaging these data. For each frequency ω , we have repeated the experiment at least four times. Hence, using Eqn. 11, we estimate the value of K for a particular ω . In addition, it is reasonable to assume that the frequency, ω , of capillary wave is the same as that of the exciter (driven by a function generator) [15]. Thus, the values of ω are found directly from the frequency readings of the function generator driving the exciter. Following these measurements, we plot a \ln - \ln graph for K *vs.* ω and evaluate the slope and y-intercept of this curve. The slope of the curve ($\frac{3}{2}$) should verify the power law predicted by the dispersion relation while the y-intercept should give the surface tension.

Our experimental results on three different liquids (water, 1-hexanol and kerosene – a mixture of petroleum hydrocarbons) are shown in Fig. 8. The non-linear least square fit (shown by lines in Fig. 8) to the data with Eqn. 9 verifies the 1.5 exponent of the dispersion

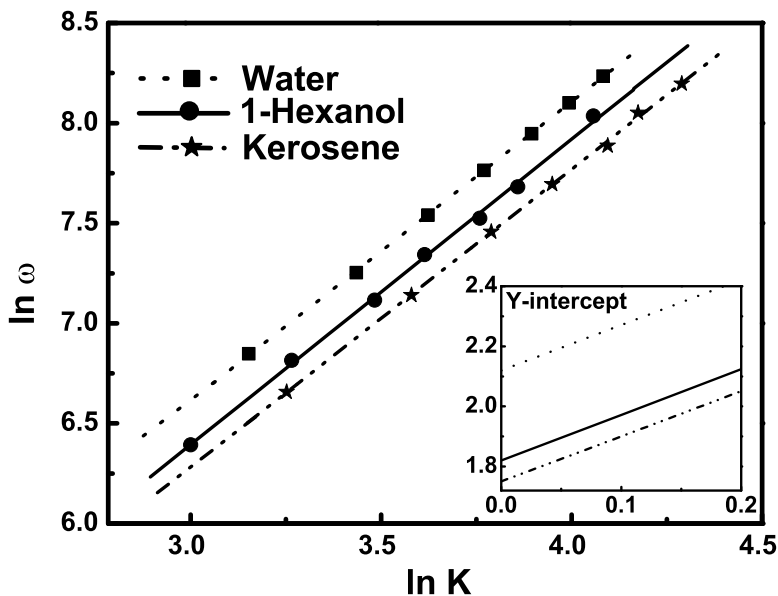


FIG. 8: The $\ln\text{-}\ln$ plots of the wavevector (K) versus the frequency (ω) exhibit a straight line of slope very close to $\frac{3}{2}$ obtained for three different liquids. The inset shows the corresponding y -intercepts.

relation within experimental uncertainty (1.5 ± 0.03). Using the known value of ρ for each liquid, we estimate the value of α from the measured y -intercept of the straight lines. It is to be noted that the maximum percentage error in measuring α is limited to 6% - 8% (for different liquids) by our measurement procedure. We have tabulated the measured values of surface tension for different liquids in Table-II. These results match quite well with the standard values of surface tension for the corresponding liquids [32].

B. Viscosity

Using the same experimental set-up, we now move on towards estimating the viscosity of a given liquid. We mentioned before that for capillary waves generated by means of a single pin exciter, the amplitude of the wave at the point of oscillation is almost the same as the amplitude of the oscillating pin in a low viscous liquid [15]. However, if we imagine a radial straight line from the source of excitation (on the liquid surface), then along this line the amplitude of surface wave is gradually damped due to the viscosity of the liquid

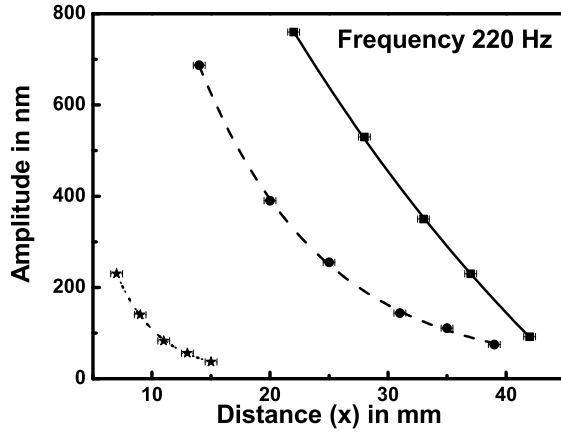


FIG. 9: Experimental plot of distance (x) versus surface capillary wave amplitude (h). Solid line, dashed line, and dotted line for the liquids water, kerosene, and 1-hexanol respectively.

(see Fig. 7). The laser beam is focused along a radial line at different distances on the liquid surface from the point of excitation (x in Fig. 7). We have seen in Sec. II that the intensities of the diffraction spots of different orders depend only on the amplitude of the capillary wave, if other parameters like θ_i and λ are kept constant (Eqn. 2). By comparing our experimentally measured intensity ratios of different orders in the diffraction pattern with those obtained from the theoretical plot (Fig. 2), we estimate the average value of h at a particular location on the liquid surface. In Fig. 9, we plot x , the distance from the point of oscillation *vs.* h , the capillary wave amplitude for three experimental liquids (water, kerosene, and 1-hexanol). We fit the data points with an exponential decay function, where we kept the decay constant (also known as spatial damping coefficient of the liquid), δ , as varying parameter. The values of δ for three different liquids are tabulated in Table-II.

The wavevector for a wave of fixed real frequency, ω , has a small imaginary part, which contributes to the spatial damping. Substituting $K = K_0 + i\delta$ (where $\delta \ll K_0$) in the well-known Navier-Stokes equation for waves on a liquid-air interface, one gets[22, 33],

$$\delta = \frac{4\eta\omega}{3\alpha}, \quad (12)$$

where η is the viscosity of the liquid. Experimentally, we have obtained the values of α and δ for the above mentioned liquids. The estimated value of viscosity of different liquids, using Eqn. 12, are shown in Table-II. The experimental plots in Fig. 9 are for frequency 220 Hz.

We have also checked our results for two other frequencies (260 Hz and 300 Hz) and have obtained similar results (see Table-II).

V. LIQUID FILMS ON LIQUIDS: THEORY AND EXPERIMENTS

Till now we have been exclusively concerned with waves on the surface of a single liquid, or, more precisely, waves at the liquid-air interface. A more complicated scenario arises when there exists a film of a different liquid on top of a given liquid (the two liquids are immiscible). In such a situation, the dispersion relation changes drastically, which, in turn, changes the surface wave profile. We now investigate the novelties that arise through studies with our optical probe.

A. Background theoretical framework

The dispersion relation in Eqn. 8 for capillary wave propagation on liquid surfaces is valid only when the depth of experimental liquid is large. For lower values of the depth of the liquid (denoted by, say y), the relation becomes [30]

$$\omega^2 = \frac{\alpha K^3}{\rho} \tanh(Ky) \quad (13)$$

where, here too, we neglect a term due to gravity. Typically, if we choose $y = 1$ cm and a range of K from 20 to 80 cm^{-1} (as used in our earlier experiment), $\tanh(Ky)$ is nearly unity, and the dispersion relation reduces to the one given by Eqn. 8. The interesting problem we focus on now is that of wave propagation on a liquid film spread out on another liquid. If the thickness of the film is very low, then not only the surface tension but also the interfacial tension across the liquid-film boundary, play a role in the propagation mechanism of the waves. We first work out a general dispersion relation where the surface and interfacial tensions as well as the film thickness appear explicitly in our mathematical expressions.

Fig. 10 shows the symbols used to represent various parameters in the following discussion. We denote the density of the lower liquid by ρ while α is the interfacial tension at the liquid-liquid interface. The same quantities for the film-air interface are represented with primes i.e., ρ' and α' respectively. The equilibrium plane of separation (interface) between the liquids is at $y = 0$. The liquid below the $y = 0$ plane extends upto a value $y = -H$

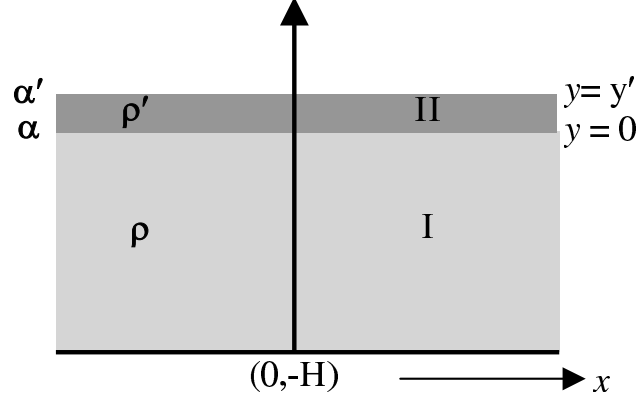


FIG. 10: Liquid film on liquid and the various parameters used.

with H being very large. The film is located above $y = 0$ with a thickness $y' \ll H$. Under these assumptions, the general expressions for the surface capillary waves in the region (I): $-H \leq y \leq 0$ and in region II : $0 \leq y \leq y'$ are given by [30],

$$\psi = Ae^{Ky} \cos(Kx - \omega t) \quad (14)$$

and

$$\psi' = [Be^{-Ky} + Ce^{Ky}] \cos(Kx - \omega t), \quad (15)$$

respectively. Here A, B and C are arbitrary constants. The above two waves must obey the following boundary conditions arising from the continuity of the velocity component (v_y) and that of pressure at the surface of separation of the two liquids, i.e.,

$$\frac{\partial \psi}{\partial y} = \frac{\partial \psi'}{\partial y}, \quad (16)$$

$$g\rho \frac{\partial \psi}{\partial y} + \rho \frac{\partial^2 \psi}{\partial t^2} - \alpha \frac{\partial}{\partial y} \left(\frac{\partial^2 \psi}{\partial x^2} \right) = \rho' \left(\frac{\partial^2 \psi'}{\partial t^2} \right) + g\rho' \left(\frac{\partial \psi'}{\partial y} \right), \quad (17)$$

$$\rho' g \frac{\partial \psi'}{\partial y} + \rho' \frac{\partial^2 \psi'}{\partial t^2} - \alpha' \frac{\partial}{\partial y} \left(\frac{\partial^2 \psi'}{\partial x^2} \right) = 0. \quad (18)$$

Evidently, the first two conditions apply at $y = 0$ while the third one is valid at the top surface at $y = y'$. In the boundary conditions above, we neglect the effect of gravity in all calculations below. Using Eqn. 14 and Eqn. 15 in Eqn. 16 and Eqn. 17 we obtain

$$A = C - B \quad (19)$$

and

$$C = B \frac{[\alpha K^3 - (\rho + \rho') \omega^2]}{[\alpha K^3 - (\rho - \rho') \omega^2]}. \quad (20)$$

Substituting Eqn. 19 and Eqn. 20 in Eqn. 18 with $y = y'$, we construct a quadratic equation for ω^2 given by:

$$\omega^4 [1 + r \tanh(Ky')] - \omega^2 [\omega_s^2 \tanh(Ky') + r\omega_s^2 + \omega_i^2] + \omega_s^2 \omega_i^2 \tanh(Ky') = 0, \quad (21)$$

where, we have used the notations $\frac{\rho'}{\rho} = r$, $\frac{\alpha' K^3}{\rho'} = \omega_s^2$ and $\frac{\alpha K^3}{\rho} = \omega_i^2$ for simplicity. The two roots of Eqn. 21 are the new dispersion relations for our given problem. The two roots are

$$\omega_{\pm}^2 = \frac{P \pm \sqrt{G}}{2Q}, \quad (22)$$

where, $P = r\omega_s^2 + \omega_s^2 \tanh(Ky') + \omega_i^2$, $Q = 1 + r \tanh(Ky')$, and $G = P^2 - 4Q\omega_s^2 \omega_i^2 \tanh(Ky')$.

Consider two limiting cases of the above dispersion relation. Let us first assume $y' \rightarrow \infty$. Then $\omega_{\pm}^2 \rightarrow \omega_s^2$ and $\omega_{\pm}^2 \rightarrow \frac{\omega_i^2}{1+r} = \frac{\alpha K^3}{\rho+\rho'}$. Thus, when y' is very large, the ω_+ mode corresponds to the waves propagating on the upper liquid surface (thus called surface mode). On the other hand, the ω_- mode involves the interfacial tension [30] as well as the density of the lower liquid and may be termed as an interface mode. In such a situation (y' large), reflecting the probe laser beam off the surface wave profile on the liquid film, we can obtain information (through the diffraction pattern) on wave propagation and properties of the liquid film. The existence of the other mode can be confirmed (for y' large) only if we perform experiments in transmitted light, though it is not clear how such information may be obtained. On the contrary, assuming $y' \rightarrow 0$ (very thin film), we get $\omega_{\pm}^2 \rightarrow (r\omega_s^2 + \omega_i^2) = \frac{(\alpha' + \alpha)K^3}{\rho}$, and $\omega_{\pm}^2 \rightarrow 0$. Thus the ω_+ mode now depends on properties of both the liquids, (α', ρ) , as well as properties of the interface (α).

Furthermore, we can obtain the constants A , B , C and hence ψ and ψ' by assuming a value for the amplitude imparted initially at the top surface. In this way, one may obtain the amplitudes of ψ and ψ' for both the modes ω_+ and ω_- . In particular, we have noted (not demonstrated here) that the nature of variation of the amplitudes of ψ' (with the film-height $0 < y' < h$) for the ω_+ mode is quite different from that for the ω_- mode. In the former case (ω_+) the value of the amplitude drops to a much smaller value at the interface compared to the drop in the amplitude for the ω_- mode. However, it is not possible for us to check this fact through our experiments. Hence we refrain from discussing this aspect further in this article.

B. Experiments and results

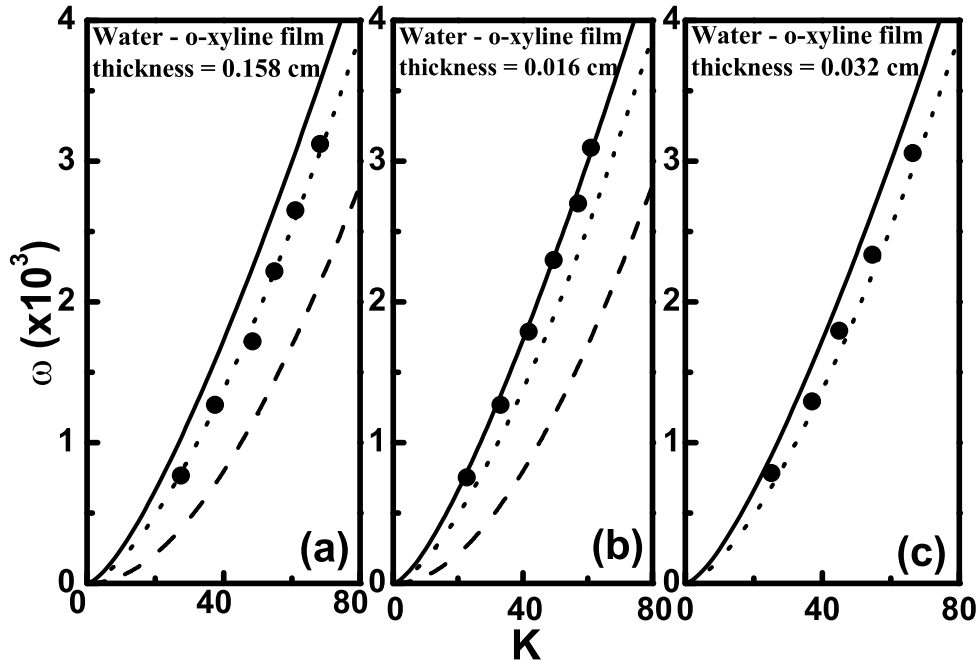


FIG. 11: Theoretical plot of frequency (ω) versus wavevector (K) for different modes in water-o-xylene liquid-liquid film at film thickness (a) 0.158 cm, (b) 0.016 cm and (c) 0.032 cm. The solid line is for ω_+ mode, dashed line is for ω_- mode and dotted line is for ω_s mode. The experimental data points are shown by the filled circles.

In our experiments, we have tried to figure out which of the two different modes (discussed in previous section) that arise due to the presence of films of kerosene, n,n-dimethyl aniline, or o-xylene spread on the surface of water, is actually present. The choice of these liquids is due to the fact that these are immiscible with water, have density lower w.r.t. water, are low-viscous and have a higher boiling point. In these experiments with films, a petridish of area $\sim 63 \text{ cm}^2$ is filled with water to a depth of nearly 1 cm and the liquid film is formed by adding a measured quantity of the second liquid in drops from a micropipette. The thickness of the film is estimated from the known volume of the liquid and the surface area of the petridish. Uniformity of the films on the water surface has been checked optically. In order to avoid any decrease in thickness due to evaporation, we have taken observations

within 5 minutes of the formation of the uniformly spread film. The measurements are of the same type as those mentioned while studying surface tension (discussed in the earlier section) except that, in the present case, we do the experiments for varying film thicknesses. Here, we show our experimental results only for o-xylene films of different thicknesses on water. For films of the other liquids mentioned above, on water, we have observed similar behavior.

To find out the mode which is present on the film surface for a liquid-film of o-xylene on water, we first plot the experimental $\omega \sim K$ behavior with film thickness as a parameter. The theoretically obtained ω - K curves for different modes : ω_+ , ω_- , and ω_s (as a limiting case of ω_+ mode) - are then placed on the same graph for comparison. Here we use standard values : $\alpha = 37.2$ dyne/cm, $\alpha' = 29.8$ dyne/cm, $\rho' = 0.88$ gm/cc, and $\rho = 1$ gm/cc in Eqn. 22 [32]. It is evident that for a film of thickness as low as 0.016 cm, the measured data corresponds to ω_+ mode [Fig. 11(b)], while for films of thickness typically 0.158 cm, the experimental data matches well with the ω_s mode [Fig. 11(a)]. However, any intermediate thickness between 0.016 and 0.158 cm yields data within the ω_+ and ω_s modes [Fig. 11(c)]. This clearly shows that the ω_+ mode always dominates over ω_- mode. For thicker films the ω_+ mode coincides with ω_s mode, whereas for thinner films the mode is still ω_+ , though it is modified by the presence of the interfacial tension and the density of the lower liquid and is not equal to ω_s .

The above conclusions have been further verified by analyzing the experimental data for the estimation of the surface and interfacial tension. We have fitted our experimental data of water-o-xylene film of thickness 0.016 cm with ω_+ and ω_- modes in Eqn. 22 by nonlinear curve fitting (keeping surface tension and interfacial tension as varying parameters). The ω_+ mode fits with the experimental data and estimates the values of surface tension (α') of o-xylene as (29.5 ± 3.6) dyne/cm and the values of interfacial tension (α) as (33.2 ± 8.8) dyne/cm [solid line in Fig. 12]. These values are very close to the standard values available in the literature [34]. On the other hand, ω_- mode fails to fit the experimental data well (dashed line in Fig. 12); moreover, it yields unphysical values of surface and interfacial tension. Experimental limitations, in our present set up, did not allow us to make films of thickness lower than the values quoted above.

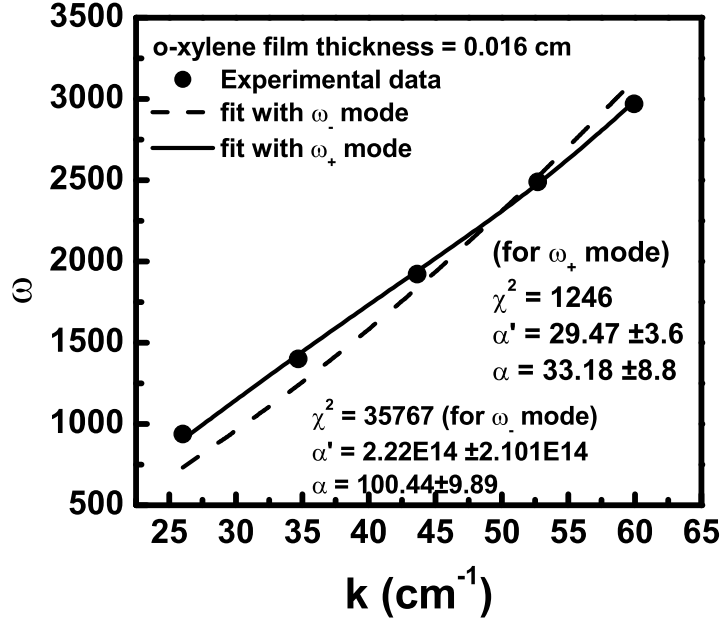


FIG. 12: Nonlinear curve fitting of the experimental data for water- o-xylene film of thickness 0.016 cm with ω_+ and ω_- modes.

VI. CONCLUDING REMARKS

In this article, we describe a simple optics-based experimental technique devised with the necessary background theoretical formulation to study the characteristics of surface capillary waves on liquids. Firstly, we visualize the profile of the surface waves using simulations with realistic values for the parameters involved. The locations of the nodes and antinodes which appear in the simulated profile are used to match the profile with actual experiments. We also claim that this combined method of simulation and experimentation can be used for other geometric configurations of oscillating sources on liquid surfaces. Subsequently, the two key liquid properties, surface tension and viscosity, which appear in the dispersion relation and play an integral role in the propagation of such capillary waves on a liquid surface, are measured optically using Fraunhofer diffraction of laser light. We note, in particular, the novelty and simplicity in the measurement of viscosity and the fact that our measurement tools, are non-destructive but by no means, less precise. Results of our experiments with several liquids, when compared to the respective values known from other

sources and literature, summarily establish the efficacy and accuracy of our approach. We anticipate, in future, the introduction of technological sophistications in our set-up, which might lead to an ‘Optical Surfacetensometer cum Viscometer’. The advantage of having a single set-up for measuring both these properties need not be further emphasised. Finally, we investigate, both experimentally and theoretically, an interesting aspect of capillary wave characteristics involved with a liquid film placed on the surface of an immiscible liquid. The dispersion relation we frame to study this case not only explains the features of the surface and interfacial modes, but also provides an estimate of the interfacial tension across the film-liquid boundary. In summary, our experimental and theoretical results seem to demonstrate the capability of our set-up in carrying out studies pertaining to capillary wave profile, liquid properties and waves on liquid films on liquids. Despite its limitations, the wide variety of information which can be obtained from such a simple set-up, makes it a tool worth improving upon in future investigations.

VII. ACKNOWLEDGMENT

Anushree Roy and Tarun Kumar Barik thank Department of Science and Technology (DST), New Delhi, India, for financial support. TKB also thanks Dibyendu Chowdhury, an undergraduate student of Vidyasagar University, West Bengal, India, for his help while doing some of the experiments.

-
- [1] G. Weisbuch and F. Garbay, “Light scattering by surface tension waves”, *Am. J. Phys.* **47**, 355-356 (1979).
 - [2] E. Wolf (ed), *Progress in Optics*, Vol. XI, (North-Holland publishing company - Amsterdam, London, 1973), pp. 125-165.
 - [3] D.P. Morgan, “A history of surface acoustic wave devices”, *Int. jou. of high speed electronics and systems* **10**, 553-602 (2000); and the references therein.
 - [4] A. Khan, R. Rimeika, D. Ciplys, R. Gaska and M.S. Shur, “Optical guided modes and surface acoustic waves in GaN grown on (0001) sapphire substrats”, *Phys. Status Solidi B* **216**, 477-480 (1999) .

- [5] C.S. Tsai, "Integrated acoustooptic circuits and applications", IEEE Trans. Ultrason. Ferroelectr. Freq.Control **39**, 529-554 (1992); and the references therein.
- [6] C. Deger, E. Born, H. Angerer, O. Ambacher, M. Stutzmann, J. Hornsteine, E. Riha and G. Fischeraurer, "Sound velocity of $Al_xGa_{1-x}N$ thin films obtained by surface acoustic wave measurements", Appl. Phys. Lett. **72**, 2400-2402 (1998).
- [7] R. Rimeika, D. Ciplys, R. Gaska, J.W. Yang, M.A. Khan, M.S. Shur and E. Towe, "Diffraction of optical waves by surface acoustic waves in GaN", Appl. Phys. Lett. **77**(4), 480-482 (2000).
- [8] P. A. Hess, "Surface acoustic waves in materials science", Physics Today, March, 42-47 (2002); and the references therein.
- [9] G.I. Stegeman, "Optical probing of surface waves and surface wave devices", IEEE tran. on sonic and ultrasonics **su-23**, 33-63 (1976); and the references therein.
- [10] J.P. Monchalin, "Optical detection of ultrasound", IEEE Trans. Ultrason. Ferroelectr. Freq. Control **33**, 485-498 (1986).
- [11] B.D. Duncan, "Visualization of surface acoustic waves by means of synchronous amplitude-modulated illumination", Appl. Opt. **39**, 2888-2895 (2000) .
- [12] F.R. Watson "Surface Tension at the Interface of Two Liquids Determined Experimentally by the Method of Ripple Waves", Phys. Rev. **12**, 257-278 (1901); F.R. Watson and W.A.Shewhart, "A study of ripple wave motion", Phys. Rev. **7**, 226-231 (1916) .
- [13] J.C. Earnshaw and R.C. McGivren, "Photon correlation spectroscopy of thermal fluctuations of liquid surface", J.Phys.**D 20**, 82-92 (1987); J. C. Earnshaw and E. McCoo, "Mode mixing of liquid surface waves", Phys. Rev. Lett.**72**, 84-87 (1994).
- [14] R. Miao, Z. Yang, J. Zhu and C. Shen, "Visualization of low frequency liquid surface acoustic waves by means of optical diffraction", Appl. Phys. Lett. **80**, 3033-3035 (2002).
- [15] T.K. Barik, A. Roy, S. Kar, "A simple experiment on diffraction of light by interfering liquid surface waves", Am. J. Phys. **73** (8), 725-729 (2005).
- [16] W.M. Klipstein, J.S. Radnich and S.K. Lamoreaux, "Thermally excited liquid surface waves and their study through the quasielastic scattering of light", Am. J. Phys. **64**(6), 758-765 (1996).
- [17] D. Walkenhorst, "Determining surface tension by light scattering", (1999), Online(28/06/05): [//www.wooster.edu/physics/JrIS/Files/Walkenhorst.pdf](http://www.wooster.edu/physics/JrIS/Files/Walkenhorst.pdf).
- [18] P.G. Klemens, "Dispersion relations for waves on liquid surface", Am. J. Phys. **52**, 451-452

- (1984).
- [19] D Langevin (ed.) *Light scattering by liquid surfaces and complementary techniques* (Marcel Dekker, New York, 1992).
- [20] I. B. Ivanov (ed.) *Thin Liquid Films, Fundamentals and Applications*, (Marcel Dekker Inc., Newyork, 1988), pp. 497-662.
- [21] V. Kolevzon and G. Gerbeth, “Light scattering spectroscopy of a liquid gallium surface”, *J. Phys. D* **29**, 2071-2081 (1996); V. Kolevzon, G. Gerbeth and G. Pozdniakov, “Light-scattering study of the mercury liquid-vapor interface”, *Phys. Rev. E* **55**, 3134-3142, (1997).
- [22] K.Y. Lee, T. Chou, D.S. Chung and E. Mazur, “Direct measurement of the spatial damping of capillary waves at liquid-vapour interfaces”, *J. Phys. Chem.* **97**, 12876-12878 (1993).
- [23] J.R. Saylor, A.J. Szeri and G.P. Foulks, “Measurement of surfactant properties using a circular capillary wave field”, *Experiments in Fluids* **29**, 509-518 (2000).
- [24] A. S. Martin, S. J. Lawrence, D. A. Rollett and J. R. Sambles, “Measurement of a Langmuir monomolecular film pressure- area compression isotherm using laser light diffracted from surface capillary waves”, *Eur. J. Phys.***14**, 19-22, (1993).
- [25] J.W. Goodman, *Introduction to Fourier optics*, (McGraw-Hill, San Francisco, 1968), p.62.
- [26] E. Hecht, *Optics*, 4th Ed. (Pearson Education) 2003, pp. 449-450.
- [27] L.I. Osipow, *Surface Chemistry*, (Reinhold publishing corporation, London), 7-21 (1993).
- [28] S.K. Ghosh, *A Text Book of Advanced Practical Physics*, (New Central Book Agency, Calcutta, 1985), pp. 62-106.
- [29] V.G. Levich, *Physicochemical hydrodynamics*, (Prentice-Hall Inc., 1962) p-596.
- [30] L.D. Landau and E.M. Lifshitz, *Fluid Mechanics*, (Pergamon press, Oxford,1975), pp. 1-44, 230-241.
- [31] L.E. Kinsler, A.R. Frey, A.B. Coppens and J.V. Sanders, *Fundamentals of acoustics*, 3rd Ed. (Wiley, New york, 1982) pp. 141-162.
- [32] D. R. Lide, *Handbook of chemistry and physics*, (CRC press , Newyork, 1998) pp. **6** 14-170.
- [33] J.A. Taylor, G.M. Lancaster and J.W. Rablais, *Appl. Surf. Sci.* **1**, 503, 1978.
- [34] D.L. Lord, K.F. Hayes, A.H. Demond and A. Salehzadeh, ”Influence of organic acid solution chemistry on subsurface transport properties. 1. surface and interfacial tension”, *Environ. Sci. Technol.* **31**, 2045-2051 (1997).

Descriptions	Angle between the lines						
	A - B	B - C	C - D	D - E	E - F	F - G	G - H
Simulated angular differences between the two corresponding minima	25.5 ⁰	18 ⁰	16 ⁰	15 ⁰	16 ⁰	18 ⁰	25.5 ⁰
Experimental angular differences between the two corresponding minima	25.1 ⁰	17.6 ⁰	16 ⁰	15 ⁰	15.7 ⁰	17.5 ⁰	25.3 ⁰

TABLE I: The simulated and experimental angular separations between the two successive destructive minima of two source interference pattern [see Fig. 2(b) and Fig. 4].

Liquids	α in dyne/cm (experimental)	α in dyne/cm (standard)	δ in cgs units	η in cp (experimental)	η in cp (standard)
Water	75 \pm 5.3	72	(0.235 \pm 0.026) (0.290 \pm 0.024) (0.304 \pm 0.031)	(0.92 \pm 0.1) at 220 Hz (0.96 \pm 0.08) at 260 Hz (0.87 \pm 0.09) at 300 Hz	0.89
Kerosene	26.3 \pm 3.7	28	(0.947 \pm 0.04) (1.11 \pm 0.05)	(1.44 \pm 0.06) at 220 Hz (1.43 \pm 0.07) at 260 Hz	1.40
1-Hexanol	28.5 \pm 3.4	26	(2.75 \pm 0.17)	(4.27 \pm 0.26) at 220 Hz	4.58

TABLE II: The experimental and standard values of surface tension (α) and viscosity (η) of different liquids at room temperature (25⁰ C). For standard values of α and η see reference [32].